Solar Hydrogen Generation from Organic Substance using Earth Abundant CuS-NiO Heterojunction Semiconductor Photocatalyst

Vempuluru Navakoteswara Rao[a], Kanakkampalayam Krishnan Cheralathan[b], Parnapalle Ravi[c], V.Jayaramakrishnan[d], Marappan Sathish[c], Sudhagar Pitchaimuthu[e]*, Murikinati Mamatha Kumari[a],Muthukonda Venkatakrishnan Shankar[a]*

[a]Nanocatalysis and Solar Fuels Research Laboratory, Department of Materials Science & Nanotechnology, Yogi Vemana University, Kadapa-516005, Andhra Pradesh, India.

[b]Department of Chemistry, School of Advanced Sciences, Vellore Institute of Technology (VIT), Vellore-632014, Tamil Nadu, India.

[c]Functional Materials Division, Central Electrochemical Research Institute (CSIR-CECRI), Karaikudi-630003, Tamil Nadu, India.

[d]Department of Engineering Physics, División of Science and Engineering, University of Guanajuato, Leon, Guanajuato, Mexico - 37150

[e]Multi-functional Photocatalyst and Coatings Group, SPECIFIC, Materials Research Centre, Faculty of Science and Engineering, Swansea University (Bay Campus), Fabian Way, Crymlyn Burrows, Swansea SA1 8EN, Wales, United Kingdom.

Corresponding Authors*

E-mail: shankar@yogivemanauniversity.ac.in (MVS)

E-mail: s.pitchaimuthu@swansea.ac.uk (SP)

Abstract

This work explores the critical role of NiO co-catalyst assembled on the surface of a CuS primary photocatalyst which effectively improves interface properties and enhances solar-to-hydrogen production by prolonging lifetime of photo-excitons generated at the CuS surface. The nanoscale CuS/NiO heterojunction is formulated using hydrothermal and wet impregnation methods. The resultant CuS/NiO composite shows optical absorbance between 380-780 nm region. The type-II energetic structure formed at CuS/NiO heterojunction facilitates rapid charge separation and as a result, the CuS/NiO composite exhibits 13 folds higher photocatalytic water splitting performance than CuO and NiO. The champion CuO/NiO photocatalyst is first identified by screening the catalysts using a preliminary water splitting test reaction under natural Sunlight irradiation. After the optimization of the catalyst, it was further explored for enhanced photocatalytic hydrogen production using different organic substances dispersed in water (alcohols, amine and organic acids). The champion CuS/NiO catalyst(CPN-2) exhibited the photocatalytic hydrogen production rate of 52.3 $mmol.h^{-1}.g^{-1}_{cat}$ in the presence of lactic acid-based aqueous electrolyte and, it is superior than hydrogen production rate obtained in the presence of other organic substances (triethanolamine, glycerol, ethylene glycol, methanol) tested under identical experimental conditions. These results indicate that the energetic structure of CuS/NiO photocatalyst is favorable for photocatalytic oxidation of lactic acid or reformation of lactic acid. The oxidation of lactic acid contributes oxidative electrons for enhanced hydrogen generation as well as protects CuS from photocorrosion. The modification of surface property and energetic structure of CuS photocatalyst by the NiO co-catalyst improves photogenerated charge carrier separation and in turn enhances the solar-to-hydrogen generation. The recyclability tests showed the potential of CPN-2 photocatalystfor prolonged photocatalytic hydrogen production while continuous supply of lactic acid feedstock is available.

Keywords: Photocatalysis; solar hydrogen; lactic acid; water splitting; metal chalcogenide

1. Introduction

In recent years, there is a growing interest in developing functional nonmaterial's useful to convert solar energy into electricity, storable chemical fuels and chemicals[1]. Utilization of solar light for overall water splitting to get H_2 and O_2 gases has been regarded as the *Holy Grail*. As molecular hydrogen (H_2),possessing high energy density has tremendous potential as a fuel in rocket engines, fuel-cell driven electric cars and hybrid motor vehicles that utilize combined hydrogen-diesel power turngreen hydrogen production is a hot research topic in energy sector[2–5]. In contrast to photoelectrochemical water splitting, solar photocatalysis in aqueous suspension is a potential approach for hydrogen production as this enables wireless water splitting; it is the one-step solution for hydrogen production utilizing earth-abundant water, renewable sunlight and non-thermal reactions carried out at near ambient temperature and pressure[6].

Consistent efforts have been put forward for the development of photocatalysts with relatively high efficiency and stability for a more extended period which may pave the way for the conversion of photocatalysis into technology for hydrogen fuel generation. In this line, developing hydrogen fuel from photo reforming of oxygenated organic compounds derived from biomass-waste or biomass-waste derived organic substrates is a process offering double benefits as it can address both energy demand and environmental clean-up simultaneously[7–10] and it is considered as a near carbon-neutral process[11]. The efficiency of hydrogen fuel generation using photocatalytic oxidation of organic substance relies on spatial separation of photogenerated electron-hole pairs[12] and surface property of the semiconductor which dictates adsorption of the targeted organic compounds[13]. The charge transfer at photocatalyst/organic substance interfaces controls the recombination loss of charge-carriers. In general, a single semiconductor could possess either surface property required for the chemical reactions or effective charge separation. Still, it is rare for a semiconductor to own both properties together. Therefore, modifying a semiconductor with appropriate material making a composite to improve adsorption of targeted compounds and spatial separation of

photogenerated electron-hole pairs concurrently is necessitated for effective hydrogen generation[14,15].

Usually, semiconductors such as simple metal oxides/sulphides/nitrides may possess required band gap of >1.23 eV, have either valence band (VB) or conduction band(CB) matching with pre-requisite energy level and rarely having favorable energetic structure needed at both VB and CB levels. However, when a semiconductor modified with a co-catalyst, it provides active sites for adsorption, suppresses excitons recombination and facilitates catalytic oxidation and reduction reactions[16,17]. For efficient photocatalytic hydrogen production, apart from suitable bandgap, band edge potential and active catalytic sites of a semiconductor, the work function of co-catalyst should match with the semiconductor for the transfer of electrons to the surface[18]. Often, a noble metal co-catalyst such as Pt is widely used (< 1 wt.%) for its high workfunction, and it provides active catalytic sites that trigger hydrogen production in manyfolds. However, the co-catalyst behavior of Pt sometimes suppressed due to preferential reaction of CO or other reaction intermediates with the active sites, this along with the higher cost of Pt lead to the search for stable and earth-abundant alternatives[19]. An alternative to Pt, several co-catalysts such as metal oxide, metal sulphides and carbon nanostructures were widely used, and in some cases, the new materials showed enhanced performance[20]. Though there are some examples for metal-chalcogenide/co-catalyst composite materials, $CdS/MoS_2@Co_{0.2}Cd_{0.8}S$ nanocomposite[21], carbon allotropes[22], $Ni_2P/ZnIn_2S_4$[23], CdS/Ni[24] and CdSe/CdS/Au@(Au-Pd alloy)[25], showed enhanced photocatalytic hydrogen production, photocorrosion of these materiels decreases the catalyst stability upon prolonged use[26].

Hence finding toxic-free metals based metal-chalcogenide alternate to cadmium and lead and identifying a suitable co-catalyst having an appropriate work function for enhanced hydrogen production will be beneficial research [27]. The copper sulphide (CuS) is a chalcogenide semiconductor meets the requirement of visible light-responsive photocatalyst but mainly used for degradation of dyes and organic pollutants. But, only a little attention has paid for its use in hydrogen production through water splitting. Recently our group extensively studied the effect of sacrificial agents on hydrogen production using CuS/TiO_2

photocatalysts[16]. On the other hand, NiO is one of the earth-abundant materials that serve as excellent co-catalysts for hydrogen generation[28]. However, a combinatorial approach on the production of CuS/NiO nanocomposite for enhanced photocatalytic hydrogen production is rare.

In the present work, we have synthesized a CuS/NiO photocatalyst and demonstrated its performance in hydrogen production via reformation of organic substances such as alcohols, amine and acids in water. The inter-dependence between properties of semiconductor and photocatalytic performance was examined and discussed. It is recognized in the work that apart from merely having favorable properties, dispersion and heterojunction interface formation between NiO and CuS surface is essential to minimize the Schottky barrier. The use of an aqueous solvent in wet-impregnation method often leads to low interface formation between CuS and NiO. Hence in the present work, we attempted polymeric surfactant mediated co-catalyst immobilization. Firstly, the CuS nanosheets are prepared using ethylene diamine as solvent as well as 2-D structure-directing agent. Then utilizing polyvinylpyrrolidone as a surfactant to mediate closer interaction, NiO co-catalyst is impregnated onto surface of CuS nanosheets. After successful catalyst preparation and its characterization, the influence of NiO co-catalyst loading and the competitiveness of the different organic substances on photocatalytic hydrogen generation performance are studied.

2. Materials and Methods

2.1 Synthesis of CuS-NiO nanocomposite photocatalyst

Analytical reagent grade chemicals procured from Fisher Scientific, India and Merck/Sigma Aldrich, India were used throughout the present work without further purification. The CuS-NiO nanocomposites wereprepared in two stages as described below.

CuS nanosheets

A simple hydrothermal method was used for CuS synthesis [16]. Briefly, 2.72 g of copper chloride ($CuCl_2.2H_2O$) (0.016 mol.) was dissolved in ethylene diamine (80 mL) in a glass beaker (capacity 100 mL) placed on a magnetic stirrer to obtain a clear solution. Into this, 2.43 g of thiourea (CH_4N_2S) (3.19 mol.) was added under vigorous stirring and then stirring continued for

another 15 min at room temperature (30±1°C). After such time, an orange coloured clear solution was obtained and the same transferred into 100 mL stainless steel autoclave having Teflon lining, and sealed with bolts and nuts. After heating in electric oven at 180±2°C for 6 h, the autoclave was cooled to room temperature under tap water flow. The black precipitate thus obtained was washed twice with 50 mL of distilled water by using dispersion and centrifugation cycles. Finally, the wet powder was washed with 50 mL of ethanol, dried in hot air oven at 80±1°C and labeled as CuS.

CuS-NiO nanocomposite

Modified wet impregnation route was adapted to disperse the NiO co-catalyst nanoparticles on CuS photocatalyst[29]. Typically, 0.5 g of Polyvinylpyrrolidone ($(C_6H_9NO)_n$ average mol. wt. 40000) was dissolved in 50 mL iso-propanol kept in a glass beaker and placed on a magnetic stirrer to obtain a colorless transparent solution. Into this, 0.5 g of CuS powder was uniformly dispersed for 15 min under ultrasonication at room temperature 30±1°C (Sol-A). In another beaker, 0.5 g of nickel nitrate ($Ni(NO_3)_2.6H_2O$) (equivalent to 20 wt% NiO loading) was dissolved in 50 mL of distilled iso-propanol in 100 mL glass beaker (Sol-B). Now, Sol-B was drop wise added into Sol-A under vigorous magnetic stirring. Into this sol-AB mixture, 30 mL of distilled water was drop wise added, and magnetic stirring continued for another 2 h at room temperature 30±1 °C. The mixture was placed on a magnetic stirrer with a hot plate and gradually heated to 120±2°C for solvent evaporation. As a result of solvent evaporation, a dark brown dry powder was obtained. The brown powder was washed with 50 mL of distilled water two times by using dispersion and centrifugation cycles. Finally, the wet powder was washed with 50 mL of ethanol and dried in a hot air oven at 80±1°C. In order to study the effect of NiO loading on CuS, the NiO loading was varied as 20, 30 & 40% and corresponding CuS-NiO nanocomposites are labeled as CPN-1, CPN-2 and CPN-3 respectively. For comparison, NiO was also prepared in using the same procedure without adding CuS.

2.2 Experimental procedure for photocatalytic hydrogen evolution

The experimental process followed for photocatalytic hydrogen evolution and processing parameters used in gas chromatography for accurate quantification of hydrogen gas was

followed as in our recent publication[29]. The pristine CuS, NiO and composite CuS/NiO (CPN-1, CPN-2 and CPN-3) were firstly tested in photocatalytic water splitting experiments under nature Sunlight irradiation. The chosen photocatalyst (pristine or nanocomposite) was dispersed rigorously in water containing 25 vol.% of sacrificial agent charged in a Quartz-Kjeldahl reactor (capacity 185 mL) placed on a magnetic stirrer and stirred strictly for 30 min to ensure adsorption-desorption process. The reactor was tightly sealed with rubber septum to ensure no gas leakage. Now, the air in the reactor was carefully evacuated by using a vacuum pump followed by purging with nitrogen gas that provided oxygen-free atmosphere. The reactor was placed on the multi-spin magnetic stirrer, and a mechanical fixture was used to hold the reactor firmly in a place at an angle of 45°; then directly exposed to nature Sunlight between 10 am to 3 pm continuously Note that these experiments are carried out under full sunny days. At periodic intervals, the reactor was brought down to the laboratory for analysis using gas chromatograph (GC) fitted with a thermal conductivity detector (TCD); the GC was calibrated with standard hydrogen and oxygen gases before the analysis of the samples obtained during the study. A similar procedure is adopted for indoor photocatalytic experiments under simulated solar light irradiation (Xenon lamp – 300 W, ORIAL Instruments, New Port Co. Ltd., USA). To calculate quantum yield, the photocatalysis experiments are performed carefully using band pass filters at 768 nm. The light intensity at this wavelength is precisely recorded using a photodiode.

The recyclability tests were carried out as follows the first cycle was performed under simulated solar light irradiation. The generated hydrogen gas was monitored at the periodic interval of one hour until 6 h. At the end of the first cycle, the reactor was wrapped with aluminum foil to avoid light entering the reactor and kept in the dark for 2 hours at room temperature 30 ±1^{o}C. Before starting the second and further recycle experiments, the reactor was evacuated (vide supra) and purged with nitrogen gas to remove H_2. The H_2 free condition was ensured by analyzing with GC. Afterwards, the reactor was exposed to light, and hydrogen produced was quantified at regular interval using the GC.

3. Results and Discussion

Both pristine (CuS) and nanocomposite (CuS-NiO) photocatalysts are synthesized through a modified procedure reported by us previously[16]. The CuS nanosheets are prepared in ethylene diamine which served as a structure-directing agent to achieve the expected morphology during the reaction of Cu^{2+} ions with thiourea. In the preparation of CuS/NiO nanocomposite, the use of polyvinylpyrrolidone creates an electrical double layer between Ni^{2+} and CuS nanosheets, which avoids the agglomeration of CuS, enables fine dispersion of NiO and aids an intimate interface formation between CuS and NiO. The prepared catalysts are thoroughly characterized to determine crystal structure, morphology, optical, optical-electrical and surface properties.

3.1 Structural and surface analysis

The powder X-ray diffraction patterns of pristine CuS, NiO and CuS/NiO composite powders are recorded at 2θ = 35 to 65° and shown in Figure 1. The CuS powder displays five major peaks appearing at 35.49, 37.48, 38.72, 43.15 and 62.84° corresponding to (101), (102), (103), (006) and (110) planes respectively. These planes are in good agreement with the Covellite phase of CuS as per standard JCPDS card No. 06-0464 and earlier reports[30]. Recently Li et al.,[31] examined 3-D CuS hierarchal structures and reported the presence of these (101), (102), (103), (006) and (110) planes of CuS. The pristine NiO showed low intensity of (111) and (200) planes probably due to its small, nanocrystalline nature leading to amorphization. Upon NiO loading, the relative peak intensity of CuS is significantly decreased while going from CPN-1 to CPN-3,even though there are no additional peaks observed.

The morphology, crystal structure and elemental composition are examined by using TEM, SAED and EDS analysis. Figure 2(a), shows nanosheets morphology of pristine CuS. The representative TEM image of CPN-2 nanocomposite is shown in Figure 2(b). The dispersion of NiO nanoparticles on the surface of the CuS nanosheets canbe visualized from the dark contrast seen in the image (Figure 2(b)). In the HRTEM image, Figure 2(c) one of the edges of the CPN-2 shows the presence of lattice fringes with d-spacing of 0.259 nm corresponding to NiO. The

lattice fringes with d spacing = 0.275 nm are associated with the (006) crystallographic plane of Covellite CuS[32], and the one with d spacing = 0.259 nm is associated with the (111) crystallographic plane of Wurtzite NiO[33].Figure 2(d) shows the SAED pattern of CPN-2. The energy dispersive X-ray analysis (EDS) spectrum of CPN-2, depicted in Figure 2 (e) confirmed the presence of elements, Cu, S, Ni, and O. The TEM analysis results clearly indicate the existence of an interface between CuS nanosheets and NiO nanoparticles.

X-ray photoelectron spectra (XPS) are recorded for investigating the chemical and electronic states of CuS and NiO present in the CPN-2 nanocomposite. The high-resolution spectrum of Cu 2p has been deconvoluted into five peaks, which appear at 962.4, 954.3, 941.8, 943.4 and 934.4 eV. Among these peaks, 954.3 and 934.4 eV are assigned to Cu-$2p_{3/2}$ and Cu-$2p_{1/2}$ which confirm the existence of copper in+2 chemical state (Figure 3(a)). There are three satellite peaks observed at 962.4, 941.8 and 943.4 eV and these peaks shifted to higher binding energy than that of Cu^{2+}, indicating strong interfacial interaction between CuS and NiO. Similar phenomenon is observed in the high-resolution S2p spectra, which features two peaks at169.2 eV (S $2p_{1/2}$) and 168.1 (S $2p_{3/2}$) (Figure 3(b)). The high-resolution spectrum of Ni 2p separated into four peaks; two 2p satellite peaks at 879.7 and 861.5 eV and two main Ni-2p peaks at 873.8 and 856.1 eV (Figure 3(c)). The lattice oxygen O1S bands of NiO are found at 531.2, and 529.3 eV Figure 3(d), indicating that they are present as O_2^-(531.2 eV) and O^-(529.3 eV) ions [34]. The similar type of functional nature of CuS/NiO heterostructures has been previously reported [35–37]. In general, the binding energy values obtained from XPS bands in this work are in good agreement with standard XPS binding energy values of Cu, S, Ni and O found in the previous reports[38].

3.2 Light absorption analysis

The recorded diffuse reflectance spectra of pristine CuS, NiO, and CuS/NiO composite range from 350 - 800 nm. The absorbance of the catalyst are normalized, as shown in Figure 4. The CuS/NiO (CPN-2) nanocomposite exhibits higher absorbance compared to CuS and NiO at 380-780 nm region. The enhanced optical absorbance of CuS/NiO (CPN-2) composite is ascribed to

the combined absorbance of CuS and NiO in the above said wavelength region. The absorbance edges of CuS and, NiO at 780 and 380.6 nm, respectively (indicated in Figure 5), reflect their bandgap energies (CuS: 1.58 eV, NiO: 3.2 eV). The normalized absorbance spectra of CuS/NiO composite powder for different loading amount of NiO (wt%) are presented in Figure S1 (supplementary information). The figure showed that the loading NiO co-catalyst onto CuS surface influences the optical absorbance of the CuS/NiO composite. Higher loading of NiO nanoparticles lead to agglomeration of NiO nanoparticles on CuS nanosheet surface and block the light received by CuS. Therefore, it is proposed that CPN-2 is the optimized catalyst and it balances the light absorption of both CuS and NiO materials.

3.3 Photocatalytic hydrogen generation

Primarily, photocatalytic performance of different NiO loaded CuS powders (CPN-1, CPN-2 and CPN-3) for hydrogen generation is tested under natural Sunlight irradiation. 25% of lactic acid dispersed in water is used as the electrolyte. Under Sunlight irradiation, the photoelectrons and photo holes generated by the primary photocatalyst, CuS are separated and go to the NiO co-catalyst and electrolyte, respectively. As lactic acid has more positive oxidation potential than water (1.3 V vs SCE), the photo holes generated at valence band of CuS can oxidize lactic acid in water and produce protons (H^+) in the electrolyte as a by-product, and provide the oxidative electrons to the valence band of CuS. Addition of these oxidative electrons to photoelectrons generated at conduction band of CuS enhances photocatalytic reduction process of protons to molecular hydrogen gas. The resultant quantities of hydrogen gas generated from pristine CuS, NiO and their composites (CPN-1, CPN-2 and CPN-3) are summarized in Figure 5a. In the Figure 5a, it can be seen that CPN-2 results in higher rate of hydrogen gas production (≈10.7 $m.mol.g^{-1}_{cat}$) compared to CPN-1 and CPN-3 as well as pristine CuS and NiO. The superior photocatalytic performance of CPN-2 composite photocatalyst might be attributed to higher photoabsorbance in the visible wavelength region than that of pristine CuS and NiO (Figure 4). Also, the formation of CuS/NiO heterojunction facilitates effective separation of photoexcited charge carriers and it may further enables transfer of electrons to

NiO. Additionally, the NiO co-catalyst is anticipated to enhance adsorption of protons, which may accelerate the photocatalytic reduction of $2H^{+} \rightarrow H_2$.

In the case of higher NiO loading (CPN-3), the excess co-catalyst present may block the surface of CuS primary photocatalyst from absorbing photons and lower the active sites required for oxidation of lactic acid. Thus the overall hydrogen gas generation rate is reduced[39]. The sustainability of CPN-2 catalyst is tested under similar experimental conditions in indoor with simulated solar light irradiation at different time intervals and results summarized in Figure 5(b). The Figure 5(a) reflects that CPN-2 can produce 42.8 $mmol.g^{-1}_{cat}$ in 4 h duration and it is sustainable.

It is known that the lifetime of photoexcitons in photocatalyst plays a key role, and it directly influences the H_2 production performance of a photocatalyst. Figure 6 displays the photoluminescence (PL) spectra of both CuS and CPN-2. The spectra show two peaks at 563 and 847 nm. The intensity of PL peaks can be correlated to charge recombination rate of photoexcitons. For instance, the lower peak intensity indicates higher charge separation, and the higher intensity represents weaker charge separation or higher charge recombination rate. Here, the lower PL peak intensity of CPN-2 indicates relatively longer charge carrier lifetime at the surface of the CuS-NiO nanocomposite catalyst. This observation is in-line with photocatalytic hydrogen production, where CPN-2 is the more efficient catalyst.

To explore the proof-of-concept of promoting solar hydrogen generation decoupling with oxidation of organic substances, the champion photocatalyst, CPN-2 is tested with wide range of organic substances such as methanol, ethylene glycol, glycerol, lactic acid and triethanolamine as mixed aqueous electrolytes (25 vol.% in water). The photocatalytic hydrogen production experiments were carried out under the optimized, identical conditions using a solar simulator as the light source. The resultant hydrogen gas quantity is summarized in Figure 7. Among the organic substances (electron donors) studied, lactic acid blended with water showed the highest hydrogen production rate of 52.3 $mmol.h^{-1}.g^{-1}_{cat}$. This result can be explained based on electron-donating property of the organic substances, which is in the

following order: lactic acid >triethanol amine> glycerol > ethylene glycol> methanol[13]**.**The schematic illustration of the proposed photocatalytic reaction mechanism on the CuS/NiO composite is presented in Figure 7 (b). As explained above, under light irradiation, the photoholes generated from the valence band of CuS will oxidize organic substance present in water. This reaction will result in providing proton and oxidative electron to CuS. The photoelectron generated at conduction band of the CuS is injected to the conduction band of NiO which reduces the protons to molecular hydrogen gas. The oxidative electrons contributed from photocatalytic oxidation of organic substance add with above-mentioned photoelectrons, which promote the overall hydrogen gas generation. Overall, the photocatalytic oxidation and reduction process relies on the energetic structure of the CuS/NiO composite, as seen in Figure 7(b). Because of it suitable electrochemical oxidation potential, lactic acid is appropriate for photocatalytic oxidation process at CuS/NiO. The electrochemical oxidation potentials of other organic substances[34] are lower than that of water oxidation potential (1.2 V vs SCE). Therefore, CuS/NiO is not able to oxidize the other organic substances studied in this work. It is another plausible reason for higher photocatalytic hydrogen generation is observed from the lactic acid-based electrolyte[40–44].

Figure 8 shows the volume of hydrogen generated for four recycles using lactic acid containing electrolyte. As noticed from the data, the volume of hydrogen produced increases with light irradiation time and the highest hydrogen production is observed at $5^{th}$and 6^{th}h. The lesser volume of gas generated at early hours of the experiment is ascribed to low hydrogen pressure; as hydrogen accumulates with irradiation time, the gas effectively releases from the reaction solution. In the 1^{st} recycle, the volume of hydrogen produced is higher, and it significantly increased from the 1^{st} hour onwards as the reaction medium consists of fresh sacrificial agent and some intermediates, which are labile and undergo oxidation to release H^+ into solution. The 2^{nd} recycle shows a similar trend as that of 1^{st} cycle but increase in gas generation recorded; subsequently, 3^{rd} recycle also proceeded in the identical way. But after 3 h, the volume of hydrogen decreased significantly may be because of formation of intermediates that limit the H^+ generation and decrease the net volume of hydrogen produced.

This negative effect is much pronounced in the 4th recycle as the volume of fresh lactic acid decreased, and the number of intermediates increased with reaction time. The net volume of hydrogen generated in the first cycle and subsequently recycles are 691, 693, 774, 324 and 314 mmol.g$^{-1}_{cat}$. The excellent stability showed by the optimized catalyst is attributed to continuous utilization of photon energy and incessant trapping of the excited charge carriers from CuS by NiO nanoparticles. The quantum efficiency of the champion photocatalyst,CPN-2 calculated to be 70.1% (details in electronic supplementary information).

3.4 Surface area and Turnover Frequency analysis

It is known that porosity and surface area strongly influence a material's catalytic abilities. Figure 9 displays nitrogen adsorption-desorption isotherms of CuS and CPN-3 photocatalysts[45,46]. Both the catalysts exhibit H3 hysteresis loop. The specific BET surface area of CPN-2 (5.8 m^2 /g) is about two folds lower than CuS (13.6 m^2 /g) as deposition of NiO on CuS surface minimizes its surface area. Over all the catalysts possess relatively smaller surface areas. The BET surface area values are used to calculate the Turnover Frequency (TOF) of CPN-2 for photocatalytic H_2 production by following the standard formula (1), and a TOF of 0.05607 s^{-1}obtained. The details of the calculation are presented in the supplementary information.

$$\text{Turnover Frequency (TOF)} = \frac{\text{Amount of product (mol)}}{\text{amount of catalytic active sites X Time (S)}} \quad \ldots\ldots. (1)$$

The solar-to-hydrogen generation performance of CuS-NiO composite (per hour/gram) from organic substance blended with aqueous media is summarized and compared with previous reportsby other researchers (Table 1). CuS-NiO showed competetive hydrogen productionrate compared to thatthat of pristine CuS and other composites containing ZnS,TiO_2, Pt andg-C_3N_4. Note that this is a qualitative comparison and does not mean that all the reference catalysts are tested under identical conditions.

4. Conclusions

In the present work, synthesis of CuS/NiO composite photocatalysts via a facile synthetic

process is demonstrated and the catalysts are explored for enhanced solar to hydrogen production from organic molecules dispersed in water. The NiO co-catalyst loading was optimized under natural Sunlight irradiation. The optimized NiO-CuS composite photocatalyst, (CPN-2) exhibited higher rate of hydrogen production under natural Sunlight irradiation (10.7 $mmol.h^{-1}.g^{-1}_{cat}$) than pristine CuS, and NiO tested under similar conditions. The CPN-2 was concurrently tested under simulated solar (UV-visible) light irradiation in the indoor and also with different organic molecules blended with water. The CPN-2 generates about 52.3 $mmol.h^{-1}.g^{-1}_{cat}$ hydrogen gas from lactic acid-based electrolyte. It indicates that lactic acid containing aqueous electrolyte is suitable for enhanced green hydrogen fuel production through photocatalytic oxidation process at CuS/NiO composite. The recyclability of photocatalyst tested for five cycles indicates that the optimized CuS-NiO photocatalyst is stable for long hours of reaction and suitable for sustainable photocatalytic hydrogen production. Further, the same catalyst exhibits a higher quantum efficiency of 70.1%. Apart from photocatalytic hydrogen production, characterization of crystallinity, optical absorption, morphology, excitons separation and chemical analysis of the synthesized photocatalysts were also carried out and correlated to hydrogen production activity.

Acknowledgments

Authors gratefully acknowledge the financial support from the Ministry of New and Renewable Energy (MNRE), New Delhi, India (No.103/227/2014-NT). And V.Navakoteswara Rao gratefully acknowledges Council of Scientific Industrial Research (CSIR-SRF), New Delhi, India for financial support through fellowship (09/1076(0005)/2019-EMR-1) to carryout Ph.D. program. S.P. thanks to European Regional Development Fund and Welsh Government for supporting Ser Cymru-II Rising Star Fellowship.

References

[1] X. Li, J. Yu, M. Jaroniec, Hierarchical photocatalysts, Chem. Soc. Rev. 45 (2016) 2603–

2636.

[2] J. Huang, Y. Cao, H. Wang, H. Yu, F. Peng, H. Zou, Z. Liu, Revealing active-site structure of porous nitrogen-defected carbon nitride for highly effective photocatalytic hydrogen evolution, Chem. Eng. J. 373 (2019) 687–699.

[3] Y.X. Zhang, P. Zeng, Y.X. Yu, W. De Zhang, Integration of nickel complex as a cocatalyst onto in-plane benzene ring-incorporated graphitic carbon nitride nanosheets for efficient photocatalytic hydrogen evolution, Chem. Eng. J. 381 (2020) 122635.

[4] C. Li, S. Du, H. Wang, S.B. Naghadeh, A.L. Allen, X. Lin, G. Li, Y. Liu, H. Xu, C. He, J.Z. Zhang, P. Fang, Enhanced visible-light-driven photocatalytic hydrogen generation using $NiCo_2S_4$/CdS nanocomposites, Chem. Eng. J. 378 (2019) 122089.

[5] J. Sun, L. Duan, Q. Wu, W. Yao, Synthesis of MoS_2 quantum dots cocatalysts and their efficient photocatalytic performance for hydrogen evolution, Chem. Eng. J. 332 (2018) 449–455.

[6] R. Singh, S. Dutta, A review on H_2 production through photocatalytic reactions using TiO_2/TiO_2-assisted catalysts, Fuel. 220 (2018) 607–620.

[7] J. Huang, G. Li, Z. Zhou, Y. Jiang, Q. Hu, C. Xue, W. Guo, Efficient photocatalytic hydrogen production over Rh and Nb codoped TiO_2 nanorods, Chem. Eng. J. 337 (2018) 282–289.

[8] C. Pak, J.Y. Woo, K. Lee, W.D. Kim, Y. Yoo, D.C. Lee, Extending the Limit of Low-Energy Photocatalysis : Dye Reduction,. Phys. Chem. C 116 (2012) 25407–25414.

[9] Q. Wang, S.-Z. Kang, X. Li, Y.-W. Yang, L. Qin, J. Mu, A facile preparation of crystalline GeS2 nanoplates and their photocatalytic activity, J. Alloys Compd. 631 (2015) 21–25.

[10] D. Dai, L. Wang, N. Xiao, S. Li, H. Xu, S. Liu, B. Xu, D. Lv, Y. Gao, W. Song, L. Ge, J. Liu, In-situ synthesis of Ni_2P co-catalyst decorated $Zn_{0.5}Cd_{0.5}S$ nanorods for high-quantum-yield photocatalytic hydrogen production under visible light irradiation, Appl. Catal. B Environ. 233 (2018) 194–201.

[11] W. Chen, Z.C. He, G.B. Huang, C.L. Wu, W.F. Chen, X.H. Liu, Direct Z-scheme 2D/2D $MnIn_2S_4$/g-C_3N_4 architectures with highly efficient photocatalytic activities towards treatment of pharmaceutical wastewater and hydrogen evolution, Chem. Eng. J. 359 (2019) 244–253.

[12] S. Li, M. Zhang, Z. Qu, X. Cui, Z. Liu, C. Piao, S. Li, J. Wang, Y. Song, Fabrication of highly active Z-scheme Ag/g-C_3N_4-Ag-Ag_3PO_4 (1 1 0) photocatalyst photocatalyst for visible light photocatalytic degradation of levofloxacin with simultaneous hydrogen production, Chem. Eng. J. 4 (2019) 122394.

[13] V. Maurino, A. Bedini, M. Minella, F. Rubertelli, E. Pelizzetti, C. Minero, Glycerol transformation through photocatalysis: A possible route to value added chemicals, J. Adv. Oxid. Technol. 11 (2008) 184–192.

[14] X. Wang, Z. Liu, Z. Liu, A Dumbbell $CaBi_2O_4$ Photoelectrode for Photoelectrochemical Water Splitting, ChemCatChem. 9 (2017) 4029–4034.

[15] R. Daghrir, P. Drogui, D. Robert, Modified TiO_2 For Environmental Photocatalytic Applications: A Review, Ind. Eng. Chem. Res. 52 (2013) 3581–3599.

[16] V. Navakoteswara Rao, N. Lakshmana Reddy, M. Mamatha Kumari, P. Ravi, M. Sathish, K.M. Kuruvilla, V. Preethi, K.R. Reddy, N.P. Shetti, T.M. Aminabhavi, M. V. Shankar, Photocatalytic recovery of H_2 from H_2S containing wastewater: Surface and interface control of photo-excitons in Cu_2S@TiO_2 core-shell nanostructures, Appl. Catal. B Environ. 254 (2019) 174–185.

[17] G. Wu, N. Guan, L. Li, Low temperature CO oxidation on Cu–Cu_2O/TiO_2 catalyst prepared by photodeposition, Catal. Sci. Technol. 1 (2011) 601–608.

[18] N.L. Reddy, V.N. Rao, M. Vijayakumar, R. Santhosh, S. Anandan, M. Karthik, M. V. Shankar, K.R. Reddy, N.P. Shetti, M.N. Nadagouda, T.M. Aminabhavi, A review on frontiers in plasmonic nano-photocatalysts for hydrogen production, Int. J. Hydrogen Energy. 44 (2019) 10453–10472.

[19] J. Taing, M.H. Cheng, J.C. Hemminger, Photodeposition of Ag or Pt onto TiO_2Nanoparticles Decorated on Step Edges of HOPG, ACS Nano. 5 (2011) 6325–6333.

[20] L.F. Garay-Rodríguez, S. Murcia-López, T. Andreu, E. Moctezuma, L.M. Torres-Martínez, J.R. Morante, Photocatalytic Hydrogen Evolution Using Bi-Metallic (Ni/Pt) $Na_2Ti_3O_7$ Whiskers: Effect of the Deposition Order, Catalysts. 9 (2019) 285.

[21] Z. Duan, L. Deng, Z. Shi, H. Zhang, H. Zeng, J. Crittenden, In situ growth of Ag-SnO_2 quantum dots on silver phosphate for photocatalytic degradation of carbamazepine: Performance, mechanism and intermediates toxicity assessment, J. Colloid Interface Sci. 534 (2019) 270–278.

[22] B.D. Jana, Debaprem, Twin T-graphene: A new semiconducting 2D carbon allotrope, Phys. Chem. Chem. Phys. 19 (2020) 1–8.

[23] X. li Li, X. jing Wang, J. yu Zhu, Y. pei Li, J. Zhao, F. tang Li, Fabrication of two-dimensional $Ni_2P/ZnIn_2S_4$ heterostructures for enhanced photocatalytic hydrogen evolution, Chem. Eng. J. 353 (2018) 15–24.

[24] M. Zhukovskyi, P. Tongying, H. Yashan, Y. Wang, M. Kuno, Efficient Photocatalytic Hydrogen Generation from Ni Nanoparticle Decorated CdS Nanosheets, ACS Catal. 5 (2015) 6615–6623.

[25] P.K. Jain, L. Amirav, S. Aloni, A.P. Alivisatos, Nanoheterostructure cation exchange: Anionic framework conservation, J. Am. Chem. Soc. 132 (2010) 9997–9999.

[26] E. Aronovitch, P. Kalisman, S. Mangel, L. Houben, L. Amirav, M. Bar-Sadan, Designing Bimetallic Co-Catalysts: A Party of Two, J. Phys. Chem. Lett. 6 (2015) 3760–3764.

[27] H. Park, W. Choi, M.R. Hoffmann, Effects of the preparation method of the ternary CdS/TiO2/Pt hybrid photocatalysts on visible light-induced hydrogen production, J. Mater. Chem. 18 (2008) 2379–2385.

[28] J. Zheng, Y. Liu, G. Ji, P. Zhang, X. Cao, B. Wang, C. Zhang, X. Zhou, Y. Zhu, D. Shi,

Hydrogenated Oxygen-Deficient Blue Anatase as Anode for High-Performance Lithium Batteries, ACS Appl. Mater. Interfaces. 7 (2015) 23431–23438.

[29] Nagappagari Lakshmana Reddy, Kanakkampalayam Krishnan Cheralathan, and S.M.V. Bernaurdshaw Neppolian, Photocatalytic Reforming of Biomass Derived Crude Glycerol in Water: A Sustainable Approach for Improved Hydrogen Generation Using $Ni(OH)_2$ Decorated TiO_2 Nanotubes under Solar Light Irradiation, ACS Sustain. Chem. Eng. 6 (2018) 3754−3764.

[30] R. Sahraei, S. Noshadi, A. Goudarzi, Growth of nanocrystalline CuS thin films at room temperature by a facile chemical deposition method, RSC Adv. 5 (2015) 77354–77361.

[31] Z. Li, L. Mi, W. Chen, H. Hou, C. Liu, H. Wang, Z. Zheng, C. Shen, Three-dimensional CuS hierarchical architectures as recyclable catalysts for dye decolorization, CrystEngComm. 14 (2012) 3965–3971.

[32] L. Sun, Z. Li, Z. Li, Y. Hu, C. Chen, C. Yang, B. Du, Y. Sun, F. Besenbacher, M. Yu, Design and mechanism of core–shell TiO_2 nanoparticles as a high-performance photothermal agent, Nanoscale. 9 (2017) 16183–16192.

[33] C.C. Nguyen, N.N. Vu, T.-O. Do, Recent advances in the development of sunlight-driven hollow structure photocatalysts and their applications, J. Mater. Chem. A. 3 (2015) 18345–18359.

[34] J.C. Dupin, D. Gonbeau, P. Vinatier, A. Levasseur, Systematic XPS studies of metal oxides, hydroxides and peroxides, Phys. Chem. Chem. Phys. 2 (2000) 1319–1324.

[35] V.N. Rao, S. Pitchaimuthu, P. Ravi, M. Sathish, H. Han, S.M. Venkatakrishnan, Retorting Photocorrosion and Enhanced Charge Carrier Separation at CdSe Nanocapsules by Chemically Synthesized TiO_2 Shell for Photocatalytic Hydrogen Fuel Generation, ChemCatChem. 12 (2020) 3139–3152.

[36] G. Zhou, D.W. Wang, L.C. Yin, N. Li, F. Li, H.M. Cheng, Oxygen bridges between nio

nanosheets and graphene for improvement of lithium storage, ACS Nano. 6 (2012) 3214–3223.

[37] S. Zhao, Y. Shen, P. Zhou, J. Zhang, W. Zhang, X. Chen, D. Wei, P. Fang, Y. Shen, Highly selective NO_2 sensor based on p-type nanocrystalline NiO thin films prepared by sol–gel dip coating, Ceram. Int. 44 (2018) 753–759.

[38] X. Deng, C. Wang, H. Yang, M. Shao, S. Zhang, X. Wang, M. Ding, J. Huang, X. Xu, One-pot hydrothermal synthesis of CdS decorated CuS microflower-like structures for enhanced photocatalytic properties, Sci. Rep. 7 (2017) 3877.

[39] E. Cui, G. Lu, Enhanced surface electron transfer by fabricating a core/shell Ni@NiO cluster on TiO2and its role on high efficient hydrogen generation under visible light irradiation, Int. J. Hydrogen Energy. 39 (2014) 8959–8968.

[40] H. Wang, Z. Jusys, R.J. Behm, Electrochemical oxidation kinetics and mechanism of ethylene glycol on a carbon supported Pt catalyst: A quantitative DEMS study, J. Electroanal. Chem. 595 (2006) 23–36.

[41] J.F. Gomes, C.A. Martins, M.J. Giz, G. Tremiliosi-Filho, G.A. Camara, Insights into the adsorption and electro-oxidation of glycerol: Self-inhibition and concentration effects, J. Catal. 301 (2013) 154–161.

[42] J.W. Guo, T.S. Zhao, J. Prabhuram, C.W. Wong, Preparation and the physical/electrochemical properties of a Pt/C nanocatalyst stabilized by citric acid for polymer electrolyte fuel cells, Electrochim. Acta. 50 (2005) 1973–1983.

[43] C. Chen, A.J. Bloomfield, S.W. Sheehan, Selective Electrochemical Oxidation of Lactic Acid Using Iridium-Based Catalysts, Ind. Eng. Chem. Res. 56 (2017) 3560–3567.

[44] K. Kalyanasundaram, J. Kiwi, M. Graetzel, Cheminform Hydrogen Evolution From Water By Visible Light, A Homogeneous Three Component Test System For Redox Catalysis, Chem. Informationsd. 10 (1979) 2720–2730.

[45] M. Tanveer, C. Cao, I. Aslam, Z. Ali, F. Idrees, W.S. Khan, M. Tahir, S. Khalid, G. Nabi, A. Mahmood, Synthesis of CuS flowers exhibiting versatile photo-catalyst response, New J. Chem. 39 (2015) 1459–1468.

[46] X.S. Hu, Y. Shen, Y.T. Zhang, J.J. Nie, Preparation of flower-like CuS/reduced graphene oxide(RGO) photocatalysts for enhanced photocatalytic activity, J. Phys. Chem. Solids. 103 (2017) 201–208.

Figure captions

Figure 1 PXRD pattern of CuS/NiO nanocomposite with different NiO loading on CuS.

Figure 2 HRTEM image of (a) CuS powder; HRTEM image of NiO-CuS composite powder (CPN-2) (b) measured at 20 nm and (c) measured at 5 nm; (d) SAED pattern of CPN-2 (e) EDS result of CPN-2.

Figure 3 X-ray photoelectron spectra of NiO-CuS (CPN-2) composite(a) Copper (b) Sulphur (c) Nickel (d) Oxygen.

Figure 4 Optical absorbance spectra (normalized) for CuS, NiO and CuS-NiO (CPN-2) composite powder.

Figure 5 Photocatalytic hydrogen gas generation performance of CuS/NiO nanocomposite under natural Sunlight irradiation (the experiments are carried out at sunny day) (a) Comparison of H_2 evolution rate for pristine CuS, NiO and nanocomposite photocatalysts, and (b) Optimization of NiO loading (wt%) on CuS. Note that the water containing 25 vol.% of lactic acid was used as electrolyte.

Figure 6 Photoluminescence spectra of CuS and CPN-2 powder showing lifetime of photoexcitons.

Figure 7 Photocatalytic activity of CPN-2 powder under simulated solar light irradiation (a) Rate of H_2 generation in the presence of different organic substances (water containing 25 vol.% of respective organic substance is used as electrolyte); (b) Schematic illustration of the energetic structure of CuS-NiO composite in photocatalytic hydrogen generation and organic substance oxidation under Sunlight irradiation. The electrochemical oxidation potential values of methanol (0.4 V vs SCE), ethylene glycol (0.6 vs SCE), triethanolamine (0.57-0.82 vs SCE), glycerol (0.7-0.8 V SCE) and lactic acid (1.35 V vs SCE) are referred from the literature. This values taken for respective organic substances against Pt electrode and in aqueous-based H_2SO_4 electrolyte.

Figure 8 Catalyst stability test for several cycles of photocatalysis reactions (the water containing 25 vol.% of lactic acid is used as electrolyte).

Figure 9 Adsorption-desorption isotherm of CuS and CPN-2 powders.

Figures

Figure 1

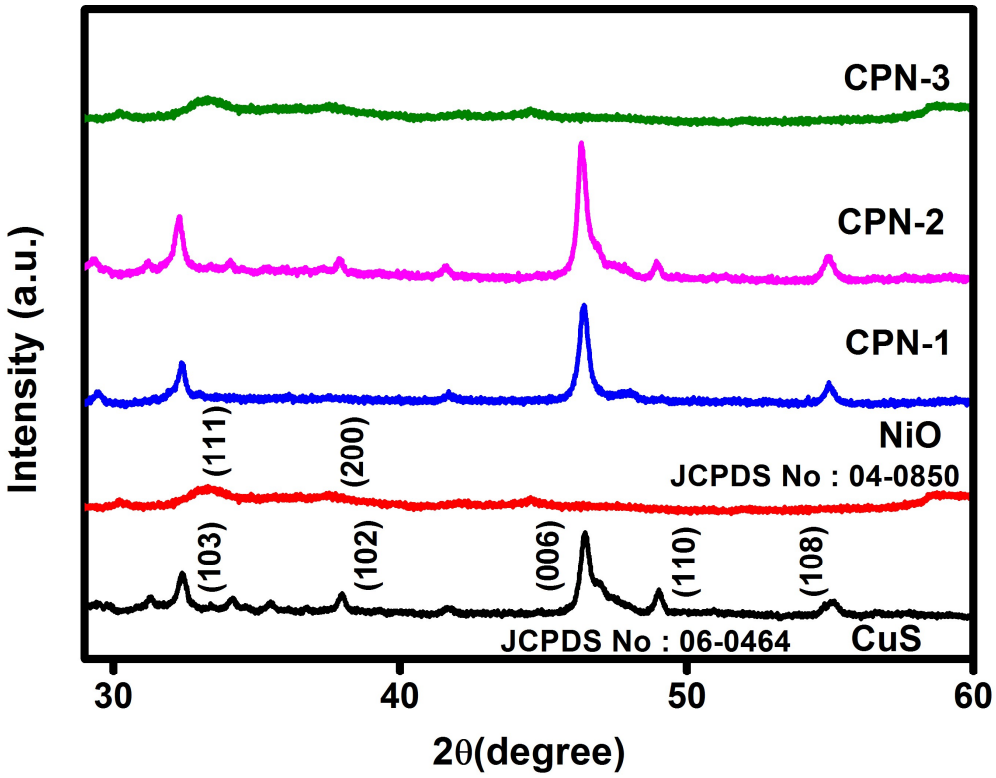

Figure 2

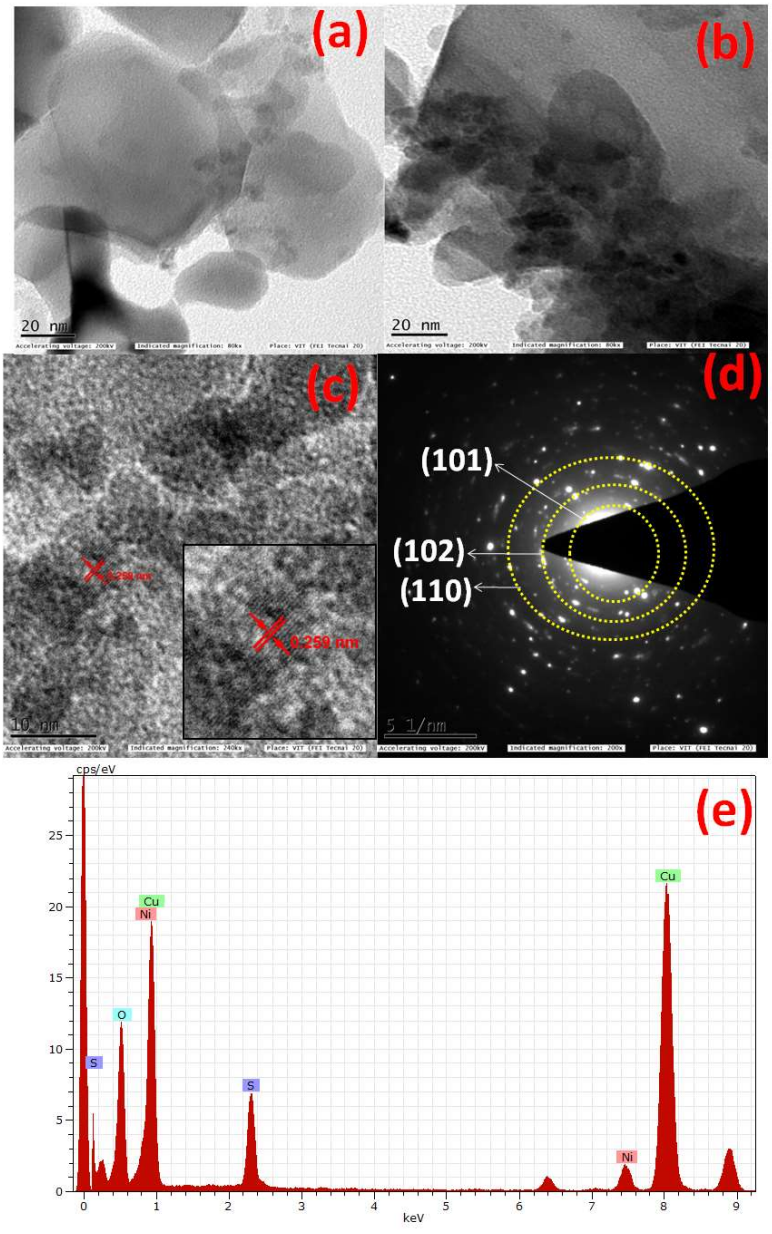
(a)
20 nm
(b)
20 nm
(c)
0.259 nm
10 nm
(d)
(101)
(102)
(110)
5 1/nm
(e)
cps/eV
Cu
Ni
O
S
S
Cu
Ni
keV

Figure 3

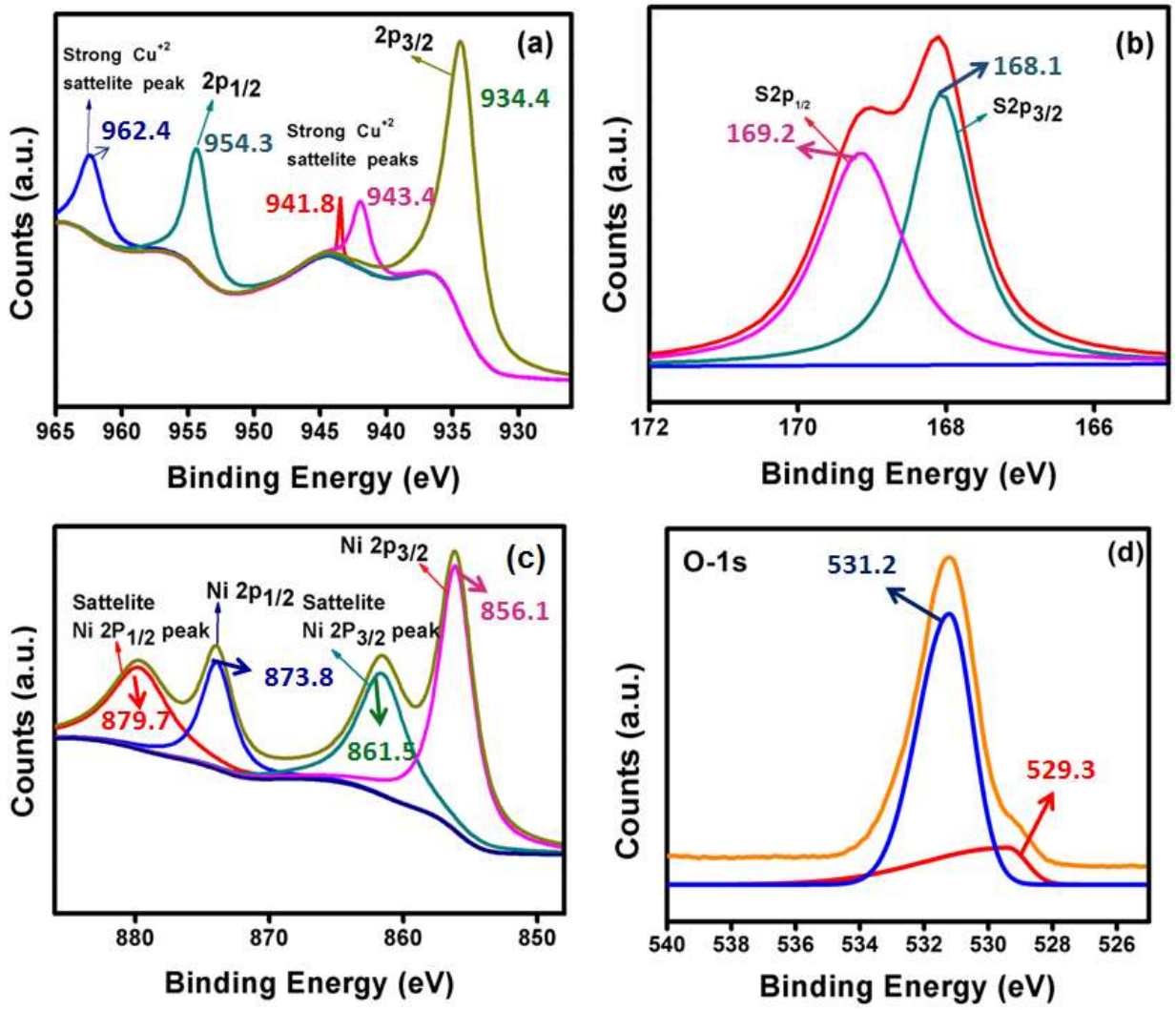
(a)
Strong Cu+2 sattelite peak
962.4
2p1/2
954.3
Strong Cu+2 sattelite peaks
941.8
943.4
2p3/2
934.4
Counts (a.u.)
965 960 955 950 945 940 935 930
Binding Energy (eV)
(b)
S2p1/2
169.2
168.1
S2p3/2
Counts (a.u.)
172 170 168 166
Binding Energy (eV)
(c)
Sattelite Ni 2P1/2 peak
879.7
Ni 2p1/2
873.8
Sattelite Ni 2P3/2 peak
861.5
Ni 2p3/2
856.1
Counts (a.u.)
880 870 860 850
Binding Energy (eV)
(d)
O-1s
531.2
529.3
Counts (a.u.)
540 538 536 534 532 530 528 526
Binding Energy (eV)

Figure 4

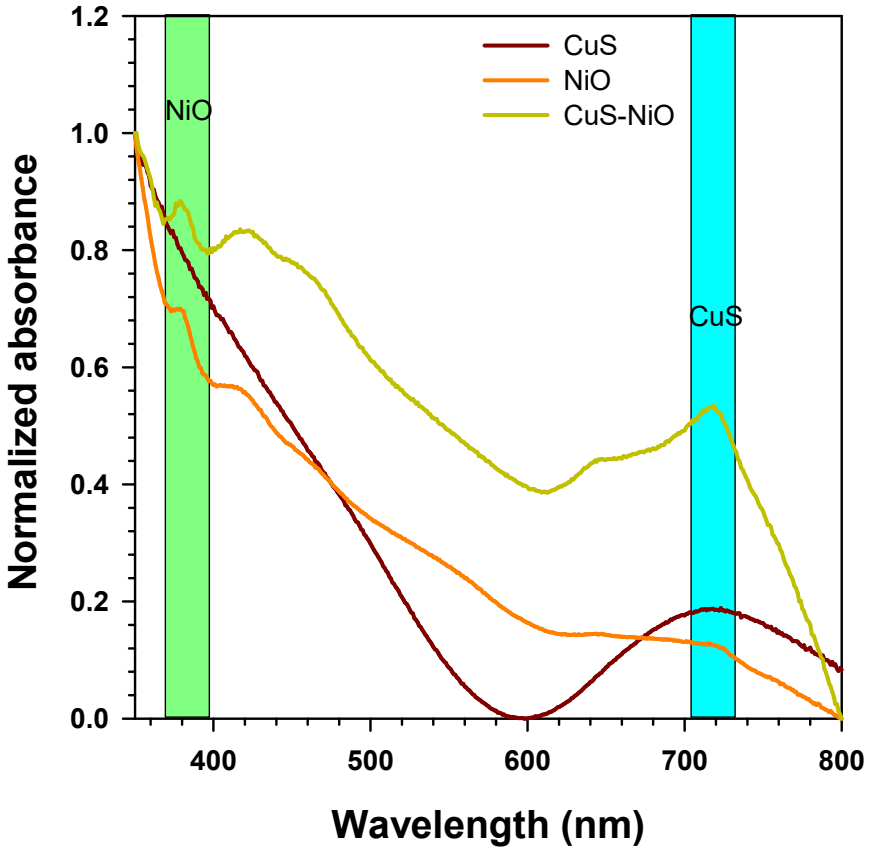
CuS
NiO
CuS-NiO
NiO
CuS
Normalized absorbance
Wavelength (nm)
0.0
0.2
0.4
0.6
0.8
1.0
1.2
400
500
600
700
800

Figure 5

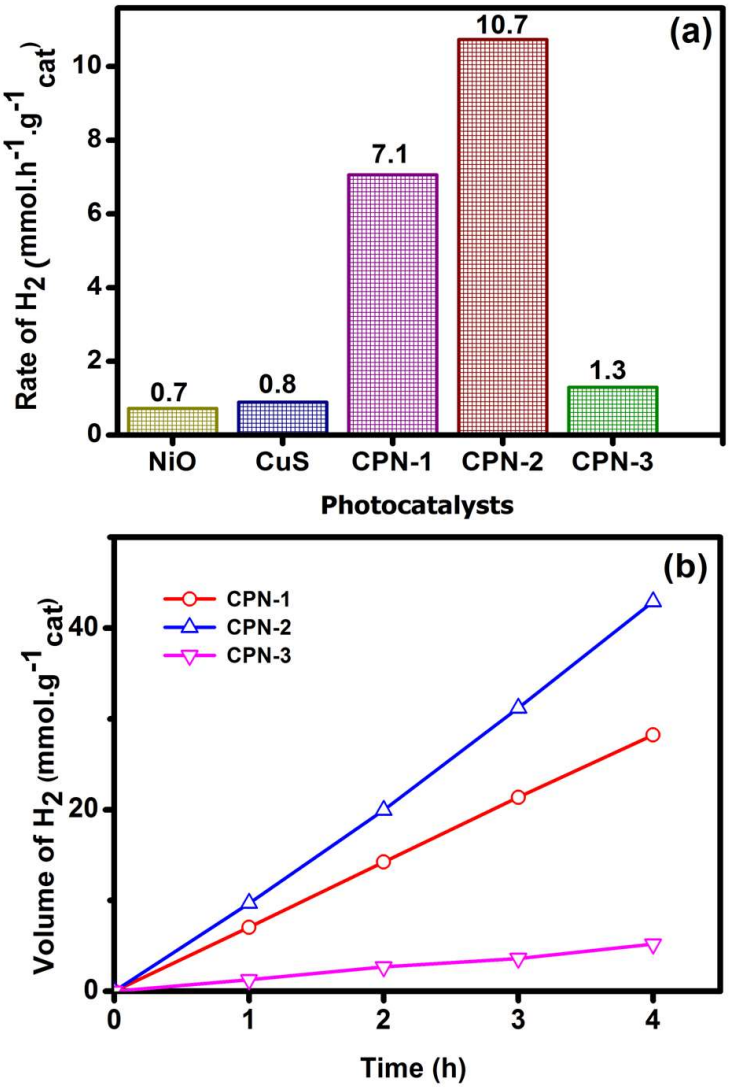
(a)
Rate of H_2 ($mmol.h^{-1}.g^{-1}_{cat}$)
0
2
4
6
8
10
0.7
0.8
7.1
10.7
1.3
NiO
CuS
CPN-1
CPN-2
CPN-3
Photocatalysts
(b)
CPN-1
CPN-2
CPN-3
Volume of H_2 ($mmol.g^{-1}_{cat}$)
0
20
40
0
1
2
3
4
Time (h)

Figure 6

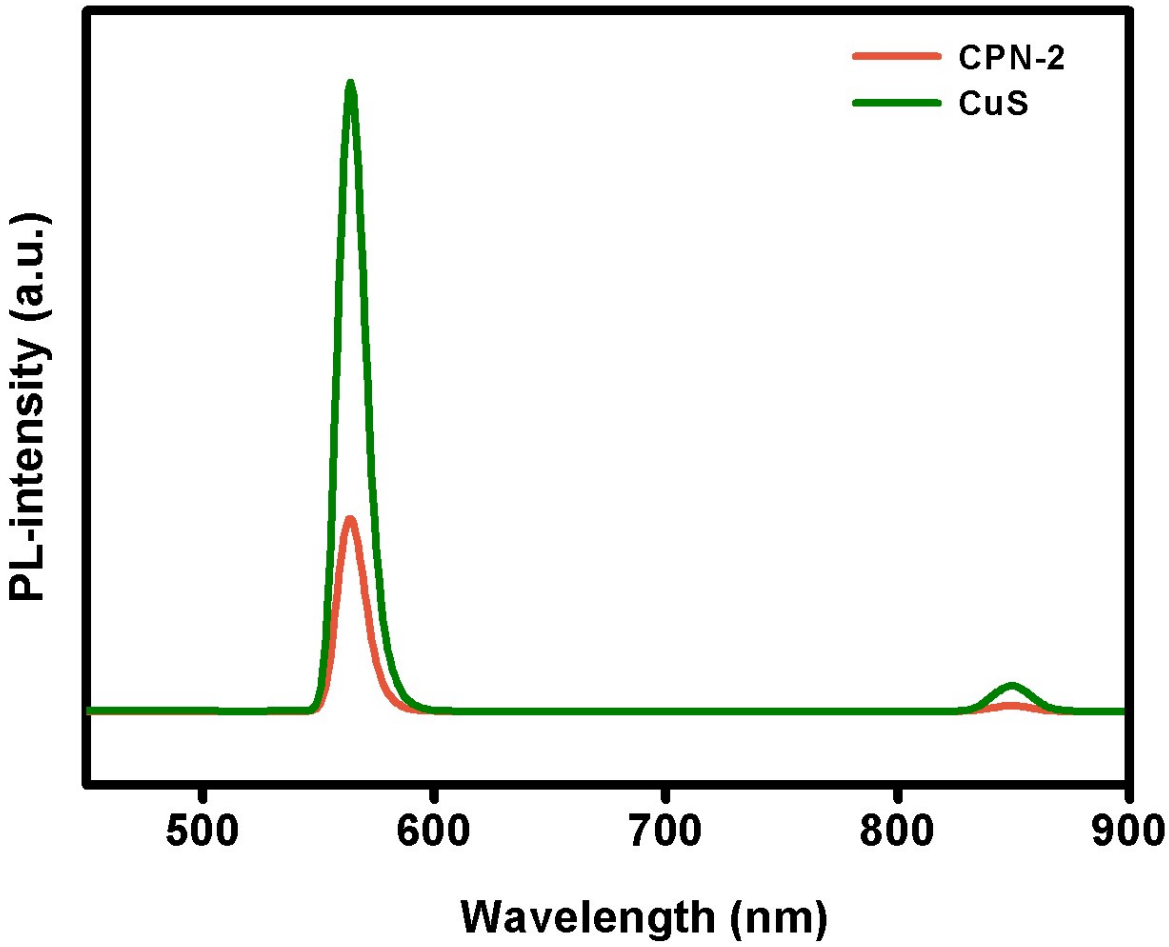

Figure 7

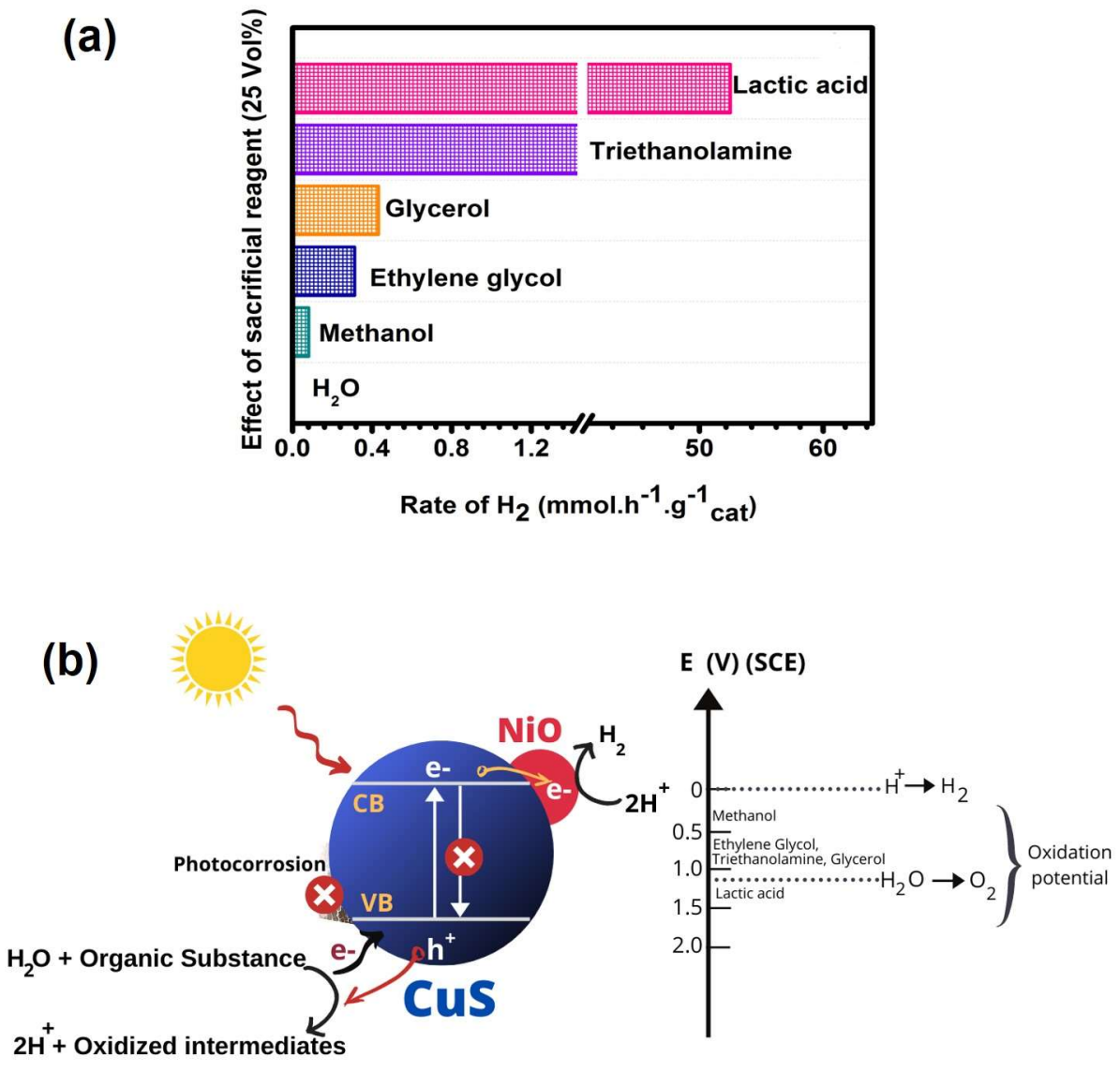
(a)
Effect of sacrificial reagent (25 Vol%)
Lactic acid
Triethanolamine
Glycerol
Ethylene glycol
Methanol
H2O
0.0
0.4
0.8
1.2
50
60
Rate of H2 (mmol.h-1.g-1cat)
(b)
E (V) (SCE)
NiO
H2
2H+
e-
CB
VB
h+
Photocorrosion
H2O + Organic Substance
2H+ + Oxidized intermediates
CuS
0
0.5
1.0
1.5
2.0
H+ → H2
Methanol
Ethylene Glycol, Triethanolamine, Glycerol
Lactic acid
H2O → O2
Oxidation potential

Figure 8

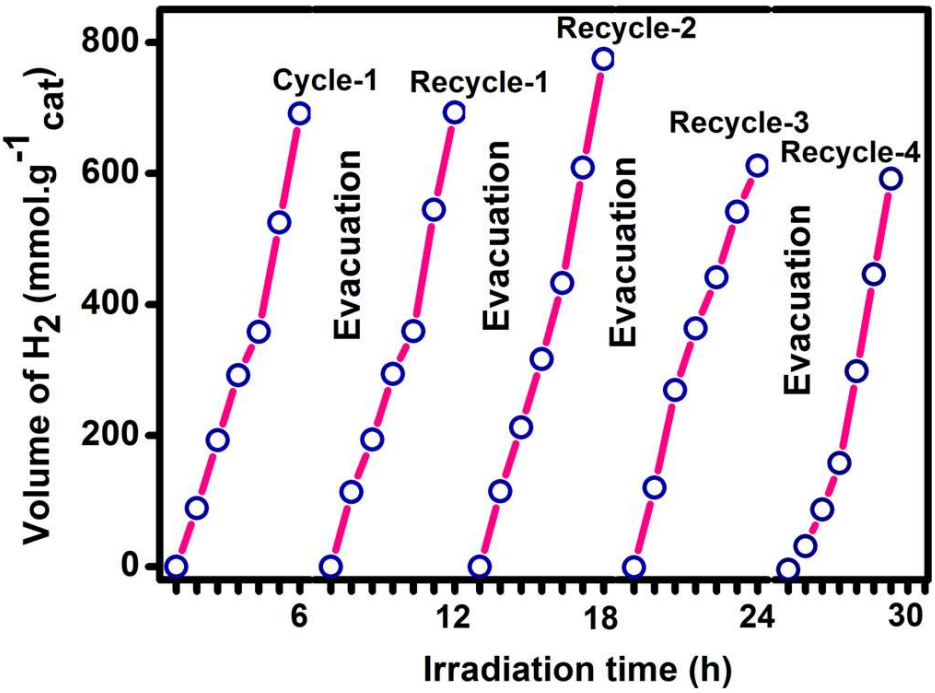
Volume of H_2 (mmol.g^{-1}_{cat})
800
600
400
200
0
6
12
18
24
30
Irradiation time (h)
Cycle-1
Evacuation
Recycle-1
Evacuation
Recycle-2
Evacuation
Recycle-3
Evacuation
Recycle-4

Figure 9

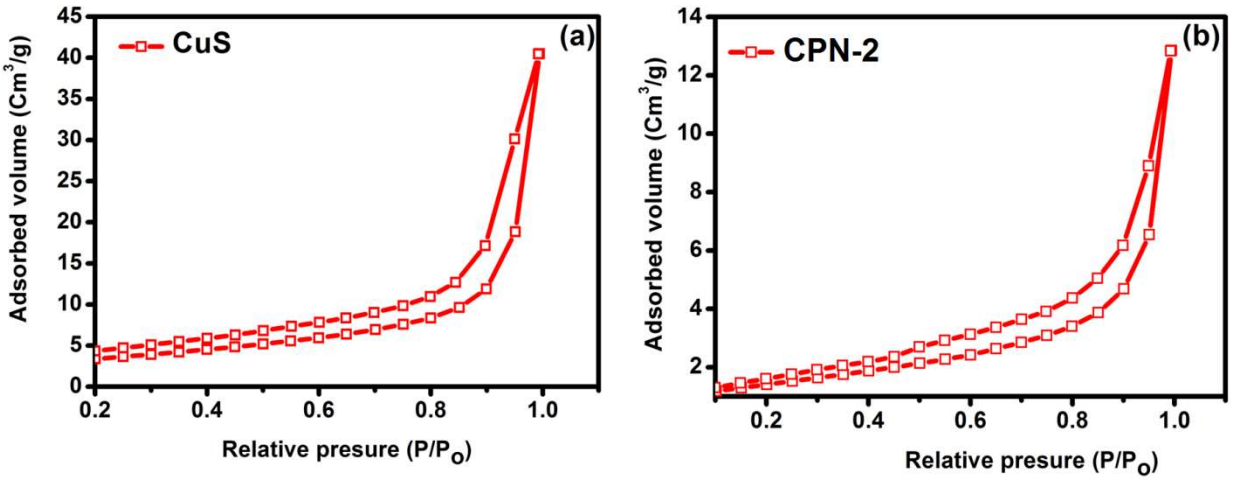
CuS
(a)
Adsorbed volume (Cm3/g)
Relative presure (P/Po)
CPN-2
(b)
Adsorbed volume (Cm3/g)
Relative presure (P/Po)

Table 1 CuS and CuS based nanocomposite photocatalysts for hydrogen production.

Sl. No.	CuS based photocatalysts	Sacrificial agent in water	Rate of H_2 production ($\mu mol.\ h^{-1}.g^{-1}$)	Light source	Reference
1.	CuS/NiO	Lactic Acid	10,742	Solar light	Present work
	CuS/NiO	Lactic Acid	52,376	Simulated Solar Light	Present work
2.	Cu_2S/ZnS	Na_2S/Na_2SO_3	2232	Visible	Michael et al, 2015
3.	CuS/ZnS	Na_2S/Na_2SO_3	4147	Visible	Zhang et a;, 2011
4.	CuS/ZnO	Na_2S/Na_2SO_3	255	Simulated Solar light	Gomathisankar et al, 2013
5.	CuS/TiO_2@Pt	Na_2S/Na_2SO_3	746	Visible	Manjunath et al, 2016
6.	CuS/TiO_2	Methanol-Water	570	UV-visible	Wang et al, 2013
7.	CuS/ZnS@g-C_3N_4	Na_2S/Na_2SO_3	9868	UV-visible	Rameshbabu et al, 2018
8.	CuS	Na_2S/Na_2SO_3	143	UV-visible	Zhou et al, 2015